The Journal of Experimental Biology 203, 741–750 (2000)
Printed in Great Britain © The Company of Biologists Limited 2000
JEB2552

OPTIMUM TAKE-OFF TECHNIQUES AND MUSCLE DESIGN FOR LONG JUMP

A. SEYFARTH[1,2], R. BLICKHAN[1,*] AND J. L. VAN LEEUWEN[2,3]

[1]*Institute for Sport Science, LSB Biomechanik, Friedrich-Schiller-University, Seidelstrasse 20, D-07749 Jena, Germany,* [2]*Neuroregulation Group, Department of Physiology, Leiden University, Wassenaarseweg 62, PO Box 9604, NL-2300RC Leiden, The Netherlands* and [3]*Experimental Zoology Group, Wageningen Institute of Animal Sciences (WIAS), Wageningen University, Marijkeweg 40, PO Box 338, 6700 AH Wageningen, The Netherlands*

*Author for correspondence (e-mail: reinhard.blickhan@uni-jena.de)

Accepted 6 December 1999; published on WWW 26 January 2000

Summary

A two-segment model based on Alexander (1990; *Phil. Trans. R. Soc. Lond. B* 329, 3–10) was used to investigate the action of knee extensor muscles during long jumps. A more realistic representation of the muscle and tendon properties than implemented previously was necessary to demonstrate the advantages of eccentric force enhancement and non-linear tendon properties.

During the take-off phase of the long jump, highly stretched leg extensor muscles are able to generate the required vertical momentum. Thereby, serially arranged elastic structures may increase the duration of muscle lengthening and dissipative operation, resulting in an enhanced force generation of the muscle–tendon complex.

To obtain maximum performance, athletes run at maximum speed and have a net loss in mechanical energy during the take-off phase. The positive work done by the concentrically operating muscle is clearly less than the work done by the surrounding system on the muscle during the eccentric phase.

Jumping performance was insensitive to changes in tendon compliance and muscle speed, but was greatly influenced by muscle strength and eccentric force enhancement. In agreement with a variety of experimental jumping performances, the optimal jumping technique (angle of attack) was insensitive to the approach speed and to muscle properties (muscle mass, the ratio of muscle fibre to tendon cross-sectional area, relative length of fibres and tendon). The muscle properties also restrict the predicted range of the angle of the velocity vector at take-off.

Key words: biomechanics, track and field, tendon, spring-like behaviour, jumping performance, human.

Introduction

Fast saltatory movements such as human running or jumping are characterised by alternating flight and contact phases. The general dynamics of the body during ground contact, represented by the centre of mass trajectory, is expressed by the pattern of ground reaction forces and determines the subsequent flight phase.

Several experimental investigations of the long jump can be found in the literature (e.g. Luhtanen and Komi, 1979; Lees et al., 1994; Stefanyshyn and Nigg, 1998). The limiting factors for attaining greater jumping distances are the ability to increase running speed (Hay, 1993) and the ability to build up large muscle forces (Alexander, 1990). A causal understanding of the contribution of different variables to jumping distance requires a mechanical model of the dynamics during the final support phase before take-off. Obviously, the long jump is a combination of a spring-like elastic operation of the leg and a hammer-like landing shock (Witters et al., 1992). An inverse dynamics approach to the running long jump (Stefanyshyn and Nigg, 1998) used only low run-up speeds, without special attention to impact dynamics. A variety of forward dynamic mechanical models have been developed for human jumps: a mass supported by a simple spring (Alexander et al., 1986; Blickhan, 1989), a two-segment model with a muscle-like torque generator (Alexander, 1990), a four-segment model with a number of muscle-like actuators (e.g. Pandy et al., 1990; Bobbert et al., 1996) and even more detailed models with many more segments and actuators (Hatze, 1981).

Our goal was to test a series of models whose components are important for describing the dynamics and optimal techniques for the long jump. In the first step, a close fit between measured ground reaction forces and the force predicted by a model was achieved (Seyfarth et al., 1999). This model, an extension of the spring-mass model of Blickhan (1989), was used to describe the spring-like operation of the supporting leg. It predicted an optimal angle of attack of approximately 45–55° for a leg stiffness of approximately $20\,kN\,m^{-1}$ and an approach speed of $10\,m\,s^{-1}$. The optimal angle decreased for a higher approach speed and increased for a higher leg stiffness, but was not much influenced by the representation of the distal mass. This model, however, did not take into account muscle properties which, to an unknown

extent, contribute to the time course of the force and may shift optimum strategies.

To investigate the role of the muscles in the long jump, the simple model of Alexander (1990) was taken as a starting point. Using a Hill-like torque generator and massless legs, his model predicted the maximum possible approach speed for the long jump to result in optimal performance. The predicted optimal angle of attack for maximum jumping performance was approximately 70–75 °. To describe the first peak in the ground reaction force, the knee extensor muscle was characterised by prestretch without eccentric force enhancement and an extremely high isometric force (approximately 25 kN). This resulted in an unrealistic sudden rise in the ground reaction force. In contrast to experimental findings, the passive and active peak were not separated by a local minimum.

In the present study, we focus on four questions. (i) To what extent is the spring-like operation of the leg due to an interaction between leg geometry and muscle–tendon properties? (ii) To what extent can a highly activated knee extensor contribute to the first force peak? (iii) What is the role of elastic components and eccentric force enhancement in jumping performance? (iv) How does jumping performance depend on muscle architecture?

To investigate these issues, a two-segment model was constructed with a Hill-type knee extensor. The extensor muscle was characterised by eccentric force enhancement and included nonlinear serial and parallel elastic components. Distal masses can easily mask the contribution of the musculature under eccentric loading and were therefore neglected in our model. Moreover, only a minor influence of a distal mass representation on the jumping technique had been found in our earlier long jump model (Seyfarth et al., 1999).

Materials and methods

Experiments

Ground reaction forces and kinematic data were recorded in an experimental analysis of 30 long jumps by 18 sports students (Seyfarth et al., 1999). The jumping distance was measured as the shortest distance between the take-off position of the foot tip and the landing point.

Model of the supporting leg

The upper and lower leg were considered as a chain of two rigid segments, each of length l and zero mass. Ground contact was assumed to occur at the distal end of the lower segment. The mass of the jumper was represented as a point mass m at the hip. The distance between the point of ground contact and the hip was the leg length l_{LEG}. The leg angle α was defined as the orientation of the leg (l_{LEG}) relative to the horizontal plane (Fig. 1).

Representation of knee extensor muscles

To describe the operation of the stance leg, at least one knee extensor muscle must be introduced (Fig. 1). The model of the muscle–tendon complex (MTC) consisted of three elements: (1) the contractile element (CE), described by a Hill-like force–velocity relationship with an eccentric force enhancement (see equations A1 and A2 in Appendix 1); (2) a parallel elastic component (PE); and (3) a serial elastic component (SE). Both elastic elements were characterised by a nonlinear stress–strain relationship (equation A4, Appendix 2). Muscle belly force $F_{CE}+F_{PE}$ was equal to the serial tendon force F_{SE}.

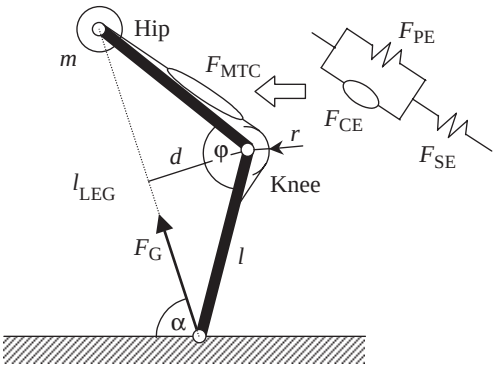

Fig. 1. The two-segment model. Each leg segment is of length l and of zero mass. The supported body is represented by a point mass m at the hip. One extensor muscle is acting at the knee joint with a constant moment arm r. Muscle force F_{MTC} is equal to the serial tendon force F_{SE} and the sum of the forces produced by the contractile element (CE) and the parallel elastic component (PE) ($F_{CE}+F_{PE}$). Leg orientation is described in terms of the leg angle α and the knee angle φ. The leg length l_{LEG} is the distance between the point of ground contact and the hip. The distance d is the moment arm of the ground reaction force F_G.

During the contact phase, the knee extensor muscle was assumed to be fully activated and had a constant moment arm r at the knee joint. The resulting torque was in equilibrium with the moment generated by the ground reaction force, F_G, with the corresponding variable moment arm d (Fig. 1, equation A5). As distal masses and the foot were neglected, the orientation of the force generated by the leg, i.e. the ground reaction force, was always identical to the leg angle α.

Initial conditions and model variables

The position of the point mass m at touch-down was described by the angle of attack α_0 and the knee angle φ_0 ($\alpha_0 \approx 60$–65 °, $\varphi_0 \approx 165$–170 °; Lees et al., 1994). For elite long jumpers, the initial velocity v_0 is approximately 10–11 m s^{-1} and has only a small vertical component (less than 1 m s^{-1}; Hay et al., 1986). For an average male athlete, we assumed a body mass of 80 kg (Luhtanen and Komi, 1979).

The height of the centre of mass is approximately 1 m for an upright standing male human 1.8 m tall (Alexander, 1990). We assumed a slightly longer leg (segment length l=0.6 m) because (1) the centre of rotation during ground contact shifts from the heel to the ball of the foot and (2) the leg (including the foot) is almost stretched at touch-down and take-off.

Muscle design

The muscle–tendon complex was represented by the

contractile element and two elastic components, a serial elastic component and a parallel elastic component (Fig. 1). Its mass m_{MTC} was not included in the calculations of the dynamics. The reference length of the muscle–tendon complex (l_{MTC}) was approximately the length of the real leg segment (0.5 m). The muscle design was described by (i) the ratio R_ℓ of the fibre length l_f to the total muscle–tendon complex length l_{MTC}, $R_\ell=l_f/l_{MTC}$, and (ii) the ratio R_A of the physiological cross-sectional area of the muscle fibres A_f to the serial tendon cross-sectional area A_t, $R_A=A_f/A_t$.

Assuming an average muscle–tendon complex density ρ_{MTC} of approximately 1100 kg m^{-3} (Spector et al., 1980; Winters and Woo, 1990), the geometry of the fibres and tendons (cross-sectional areas and lengths) could be expressed in terms of m_{MTC}, R_A and R_ℓ (equations A8 and A9, Appendix 4). The cross-sectional area of the parallel element A_{PE} accounted for a small part (1 %) of the muscle fibre area A_f, the remaining area belonging to the fibres themselves: $A_{CE}=0.99A_f$.

The maximum isometric force of the muscle fibres F_{Max} was defined assuming a muscle fibre maximum isometric stress σ_{Max} of 300 kPa (Alexander and Vernon, 1975; Close, 1972; equation A3). The maximum shortening velocity v_{Max} is the product of the fibre length l_f and the maximum fibre strain rate $\dot{\varepsilon}_{Max}$ and was assumed to be 14 l_f s^{-1} (Spector et al., 1980).

In reality, the moment arm d of the ground reaction force is much shorter than described in a two-segment model (Fig. 1). After the first 40 ms of ground contact, the centre of pressure shifts from the ankle joint to the ball of the foot. Therefore, to generate realistic values of the ground reaction force, an unrealistically high maximum isometric muscle force F_{Max} of approximately 13 kN had to be assumed (see also Alexander, 1990).

Numerical procedure

The trajectory of the point mass, given by the leg force and the gravitational force, was obtained by integrating the equations of motion (equations A6 and A7) numerically with a constant time step (0.01 ms). The calculation was terminated at the instant of take-off, i.e. when the ground reaction force became zero. The resulting jumping distance was calculated assuming a frictionless parabolic flight trajectory and landing at the intersection of the centre of mass trajectory with the ground (equation A10).

Parameter studies

The optimal angle of attack α_{opt} leading to a maximum jumping distance was investigated with respect to (i) the running speed at touch-down v_0, (ii) the total muscle–tendon complex mass m_{MTC}, (iii) the ratio of muscle fibre to serial tendon cross-sectional areas R_A, and (iv) the relative fibre length R_ℓ. During the take-off phase, maximum activation of the muscle was assumed because this resulted in the longest jumps and agrees with experimental observations (Kyröläinen et al., 1987).

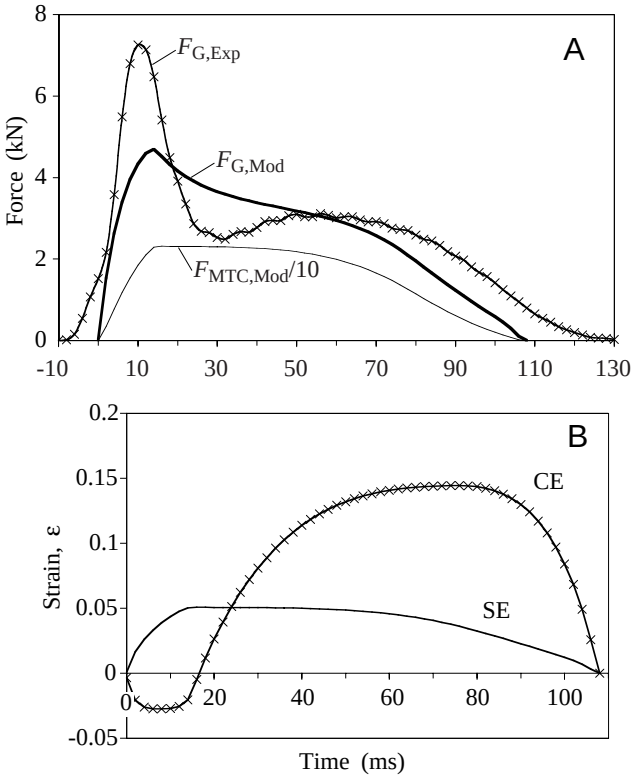

Fig. 2. Dynamics of the two-segment model. (A) Predicted ground reaction force $F_{G,Mod}$ compared with an experimentally measured value $F_{G,Exp}$ (taken from Seyfarth et al., 1999) and the predicted internal muscle force $F_{MTC,Mod}$. (B) Strain ε of the contractile element (CE) and serial elastic component (tendon; SE) during ground contact. Concentric contraction takes place only within the first 10 ms and within the last 30 ms. Lengthening of the muscle–tendon complex (MTC) is largely taken up by tendon elongation (see below: R_ℓ). Model variables (for definitions, see List of symbols), m=80 kg, l=0.6 m, m_{MTC}=4 kg, l_{MTC}=0.5 m, σ_{Max}=300 kPa, R_A=100, R_ℓ=0.16, l_f=0.08 m; initial variables, $v_{0,x}$=9 m s^{-1}, $v_{0,y}$=–0.4 m s^{-1}, α_0=60 °, φ_0=170 °.

Results

Forces and work output by muscle and leg

Fig. 2A shows an example of predicted force patterns (modelled ground reaction force $F_{G,Mod}$ and muscle–tendon complex force $F_{MTC,Mod}$) with a fully activated knee extensor muscle compared with a measured ground reaction force $F_{G,Exp}$ for a 6.9 m jump at an approach speed of 9 m s^{-1} from Seyfarth et al. (1999). This curve can be taken as an example for the other tracings. The simulated jump resulted in a jumping distance of 6.3 m, with the angle of the velocity vector at take-off being approximately 14 ° (measured angle 21 °).

No preactivation was assumed before the moment of touch-down. The general pattern of the predicted dynamics agreed with the experimental result. In both cases, a sharp rise in ground reaction force (first peak) was followed by a prolonged force at a lower level (second peak), but the two peaks were not separated by a local minimum in the simulation. In Fig. 2A, the measured force curve starts 10 ms earlier than the simulated

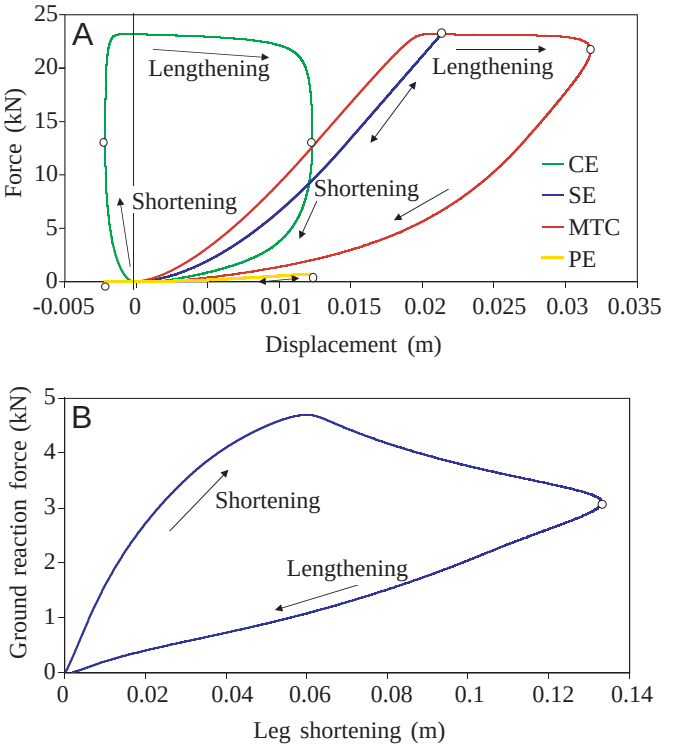

Fig. 3. Predicted work loops of (A) the muscle–tendon complex (MTC) including the contractile element (CE), serial element (SE) and parallel element (PE), and (B) the supporting leg according to the situation in Fig. 2. Leg shortening is defined as the difference between the actual leg length l_{LEG} and the leg length at the instant of touch-down. (B) During lengthening, the leg shows almost linear behaviour. The small circles in A and B represent the transitions between shortening and lengthening.

curve because there was no segment representing the foot in the model that would be decelerated first (Seyfarth et al., 1999).

The predicted muscle force had achieved its maximum value by 15 ms after touch-down, when the muscle fibres were at their maximum stretching velocity. The serial tendon had a positive strain during the whole ground contact period (SE in Fig. 2B). It was stretched rapidly immediately after touch-down, shortened very slightly over the next approximately 30 ms (plateau phase) and shortened continuously over the second half of ground contact. The muscle fibres shortened during the first few milliseconds and during the last 35 ms before take-off (CE in Fig. 2B), when the muscle force was less than the maximum isometric force F_{Max} (neglecting the force of the parallel elastic element). During most of the ground contact period (approximately 10–80 ms), the muscle fibres were lengthening and therefore absorbing energy.

Because of the large ground reaction force (up to approximately 5 kN) during the first 20 ms of ground contact, the leg showed a negative work loop (Fig. 3B). After maximum knee flexion, the path of the force–length curve was almost linear (Fig. 3B), in contrast to the nonlinear operation of the extensor muscle (MTC, Fig. 3A). The total energy lost (approximately 280 J, i.e. 44 % of the total muscle work or 9 % of the initial kinetic energy) was absorbed by the muscle fibres (Fig. 4).

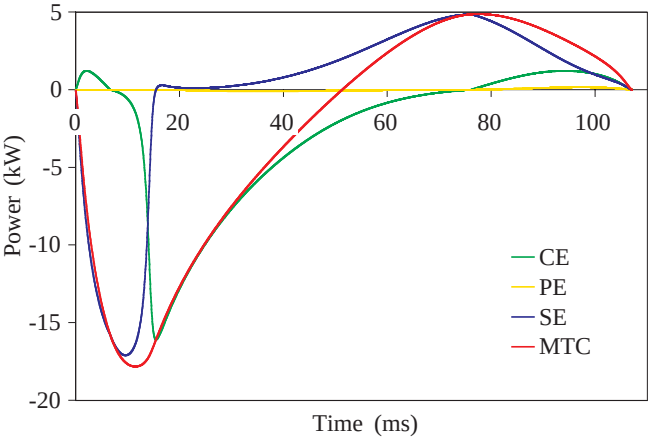

Fig. 4. Predicted power delivered by the muscle tendon complex (MTC) with the contractile element (CE), serial element (SE) and parallel element (PE). Power is largely absorbed by the tendon (SE) and the muscle fibres (CE) during the first half of the step, whereas only the tendon delivers power during take-off.

The shape of the contractile element work loop was almost rectangular (Fig. 3A). Only 8 % of the energy transferred to the contractile element was returned to the point mass during the concentric phase (Fig. 4). In contrast, in the serial elastic component, approximately 80 % of the stored energy was reusable as mechanical energy. The remainder was absorbed by the contractile element.

Optimal jumping techniques

Approach speed and angle of attack

In Fig. 5, the influence of the angle of attack α_0 and the running speed v_0 on the jumping distance, the percentage of mechanical energy of the point mass at take-off relative to that at the instant of touch-down, and the angle of the velocity vector at take-off is shown. For high approach speeds (greater than 6 m s^{-1}), the optimal angle of attack (approximately 65–70 °) was insensitive to the approach speed (Fig. 5A). The change in mechanical energy during the take-off phase was approximately ±5 % while using an optimal angle of attack (Fig. 5B). For running speeds greater than 5 m s^{-1}, optimal performance required a net loss of energy. At lower approach velocities, the leg generated net positive work for optimal performance. This required optimum angles of attack greater than 70 ° (Fig. 5B).

The angle of the velocity vector at take-off relative to the horizontal plane (take-off velocity angle, Fig. 5C) increased for decreased angles of attack if the running speed was less than 8 m s^{-1}. At higher speeds, the take-off velocity angle was insensitive to the angle of attack or even decreased slightly for small angles of attack.

The influence of the initial knee angle φ_0

Compared with the situation in Fig. 2 (initial knee angle 170 °), a smaller knee angle φ_0 led to a shorter jumping

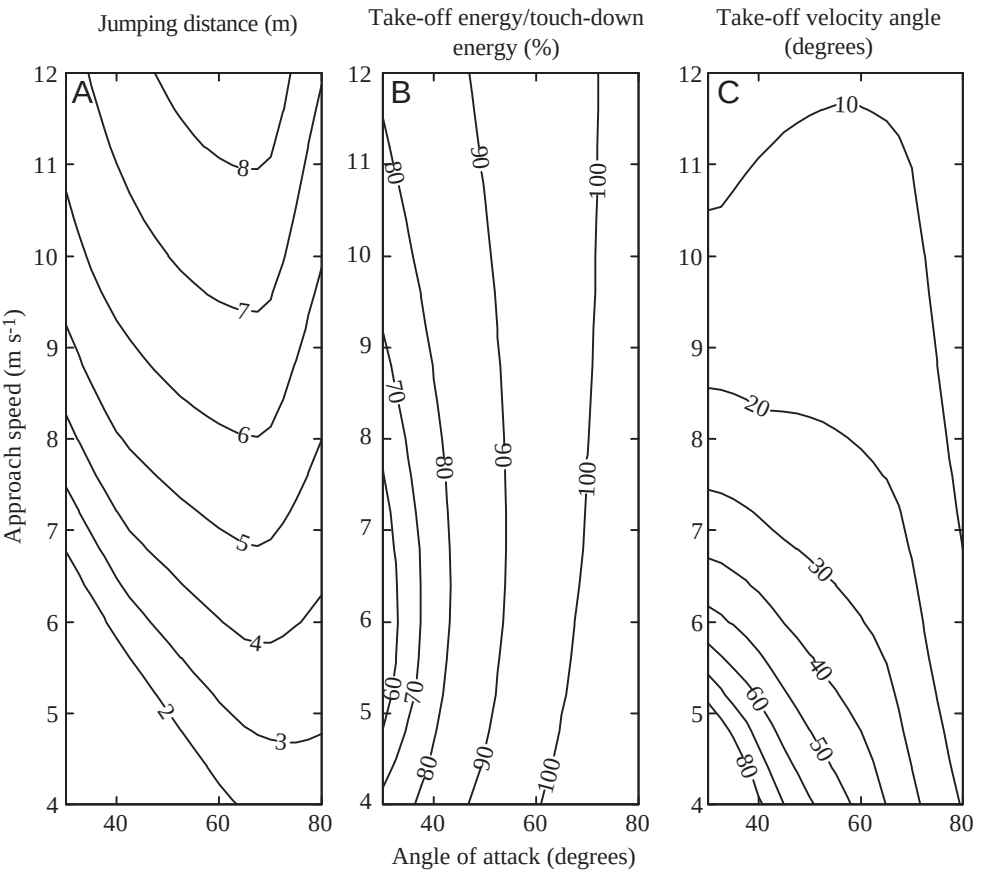

Fig. 5. Influence of the angle of attack at touch-down α_0 and the approach speed v_0 on (A) the jumping distance (contour lines, in m), (B) the percentage of take-off to touch-down mechanical energy (contour lines, as a percentage), and (C) the angle of the velocity vector at take-off relative to the horizontal plane (contour lines, in degrees). The optimal angle of attack (65–70 °) for the long jump is insensitive to the approach speed for velocities higher than 6 m s^{-1}. The optimal jumping distance (A) is achieved with nearly complete energy recovery (B). At high running speeds, only flat angles of the velocity vector at take-off can be realised (C), and flatter angles of attack do not necessarily lead to steeper take-off angles. Model variables are given in Fig. 2. In all studies, the vertical touch-down velocity was zero.

distance (for φ_0=160 ° a difference of –19 cm, and for φ_0=150 ° a difference of –38 cm) and a decreased take-off velocity angle (for φ_0=160 ° a difference of –2 °, and for φ_0=150 ° a difference of –4 °). Nevertheless, the percentage of the take-off to touch-down mechanical energy increased for smaller knee angles φ_0 (for φ_0=160 ° a difference of +1.7 %, and for φ_0=150 ° a difference of +3.2 %).

Optimal muscle design and angle of attack

The influence of the angle of attack, the total muscle mass m_{MTC}, the ratio of muscle fibre to tendon cross-sectional area R_A and the relative fibre length R_ℓ on the jumping distance is shown in Fig. 6.

Keeping the architectural variables (R_A, R_ℓ) constant, the muscle mass determined the maximum force exerted by the leg and had a strong influence on the jumping distance (Fig. 6A). For masses greater than 4 kg, the optimal angle of attack (approximately 65 °) was fairly insensitive to changes in muscle mass. Note that the muscle mass is not part of the accelerated mass, it simply represents the volume of the musculature.

For a realistic value of the muscle fibre to tendon cross-sectional area ratio of approximately 100 (Winters and Woo, 1990; Pierrynowski, 1985), the optimal angle of attack was approximately 65–70 ° (Fig. 6B). At high ratios (R_A>140) and angles of attack less than 65 °, slightly higher distances can be achieved. The muscle can produce higher forces and the tendon becomes more compliant. In contrast, for thick tendons (R_A<30), this optimum shifted to steeper angles (more than 70 °). However, the jumping performance was not much influenced by R_A.

The influence of the relative fibre length R_ℓ proved to be more complex (Fig. 6C). Very short muscle fibres (R_ℓ=0.01) led to unrealistically large jumping distances (for humans more than 9 m at an approach speed of 9 m s^{-1}) at realistic optimal angles of attack α_{opt} of 60–65 °. A relative fibre length of approximately 0.05 predicted the smallest α_{opt} of approximately 60 ° and a jumping distance of approximately 9 m. For longer fibres, α_{opt} increased. For example, at R_ℓ=0.15, a realistic jumping distance (6.7 m) with an α_{opt} of 65–70 ° was calculated.

Compared with the situation in Fig. 2, the predicted jumping distance was quite insensitive to changes in maximum shortening speed of the muscle fibres v_{Max} (less than 1 % change in distance for twice or half the original speed). Halving or doubling the tendon compliance also led to a surprisingly small change in jumping distance (less than 3 %). Thus, jumping distance is insensitive to muscle speed and to the serial tendon compliance.

In contrast, changes in the total muscle–tendon complex mass m_{MTC} (to 50 % or 200 %), of the maximum isometric muscle fibre stress σ_{Max} (to 50 % or 200 %) and of eccentric force enhancement N_{ECC} (defined as the ratio between maximum eccentric force F_{ECC} and maximum isometric force

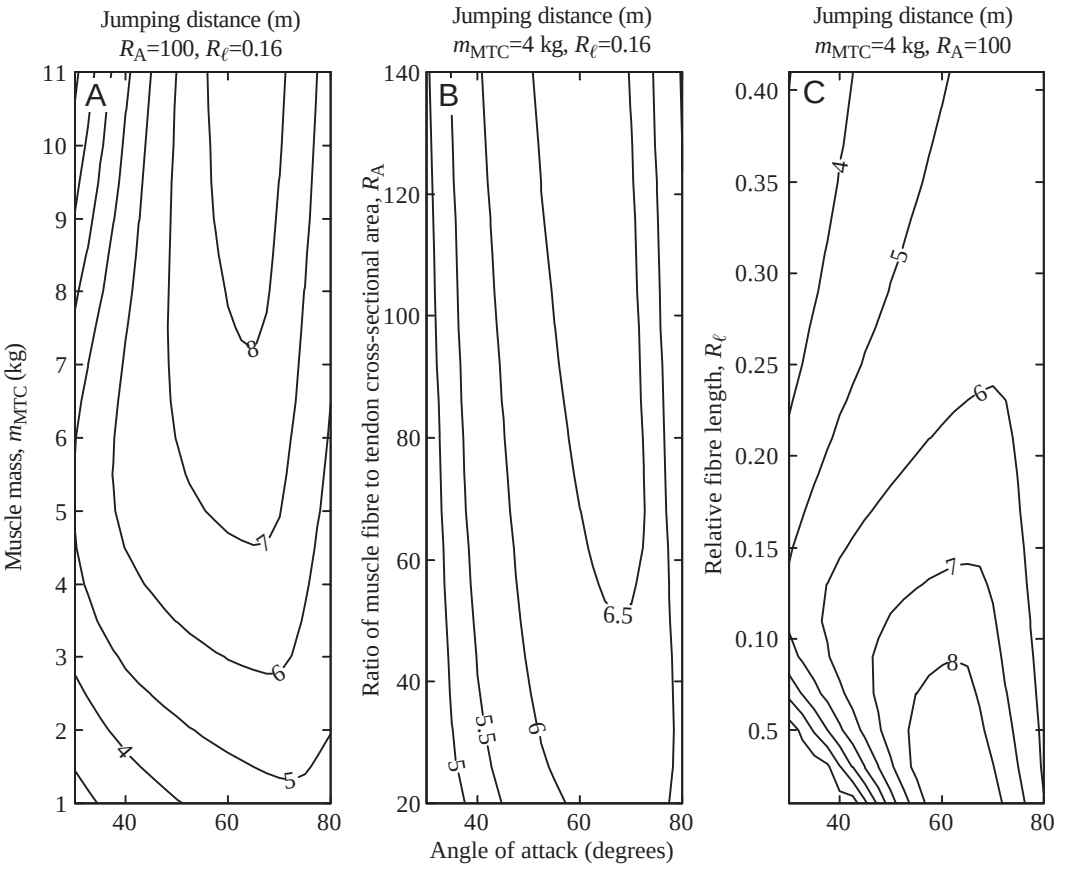

Fig. 6. Influence of the angle of attack at touch-down α_0 and (A) the total muscle mass m_{MTC}, (B) the ratio of fibre to tendon cross-sectional areas R_A and (C) the relative fibre length R_ℓ on jumping distance (contour lines, in m). Jumping distance depends strongly on muscle mass (A) and much less on the partitioning between elastic and contractile tissues (B,C). The optimal angle of attack (65–70 °) is largely insensitive to the muscle mass m_{MTC} (A), and slightly dependent on the ratio of the cross-sectional areas R_A (B) and the relative fibre length R_ℓ (C). For longer fibres (larger R_ℓ), the optimum for α_0 becomes more pronounced. Model and initial variables are given in Fig. 2. In all studies, the vertical touch-down velocity was zero.

F_{Max}; from 1.8 to 1.4 or 2.2, respectively) led to a considerable change in jumping distance (m_{MTC}, –24 % or +25 %, σ_{Max}, –22 % or +35 %, N_{ECC}, –8 % or +8 %). Thus, jumping distance is sensitive to muscle strength and to eccentric force enhancement.

Discussion

The model presented here predicted the angle of attack used in the long jump to be insensitive to running speed (>6 m s^{-1}) and muscle design. The angles agreed with the experimental observations of Seyfarth et al. (1999) within a range of approximately 5 °. Furthermore, the model gave a reasonable explanation of why long jumpers use relatively low take-off velocity angles and of the extent to which they take advantage of energy losses in leg muscle. Although the model was very simple, it provided insights into muscular dynamics at high stretching velocities and into the contribution of a fully activated knee extensor muscle to the shape of the ground reaction force over time in running and jumping.

To what extent is the spring-like operation of the leg due to an interaction between leg geometry and muscle–tendon properties?

Because of relatively short muscle fibres (R_ℓ=0.16) and high muscle activation (shown experimentally by Kyröläinen et al., 1987), lengthening of the muscle–tendon complex takes place largely within the serial tendon. Therefore, the muscle–tendon complex work loop was strongly influenced by the J-shaped nonlinear stress–strain curve of the tendon (Fig. 3A). The geometry function, given by the ratio of ground reaction force to muscle–tendon complex force, was high for an almost stretched knee joint exactly at the instant at which tendon stiffness was low (for small deflections). Furthermore, during muscle shortening before take-off, the maximum force decreased continuously with increasing shortening velocity. This resulted in an almost linear region of the work loop during unloading (Fig. 3B). The region of linear behaviour could be extended by elastic components in other leg muscles with more compliant tendons (e.g. the Achilles tendon) or by reducing the muscle activation just before the active peak, as observed experimentally (Kyröläinen et al., 1987), and it may simplify the control of jumps.

In contrast to a spring-mass system with a constant leg stiffness (Seyfarth et al., 1999), a realistic muscle automatically adapts its stiffness at different leg shortening velocities, which keeps the optimal jumping techniques robust (Fig. 7). Characterisation of this effect requires a proper description of the muscle eccentric force enhancement together with suitable compliance characteristics of the serial elastic tendon.

Taking the force–length relationship of the knee extensor into account (Fig. 7), the spring-like behaviour of the leg would be slightly enhanced. Depending on the initial fibre

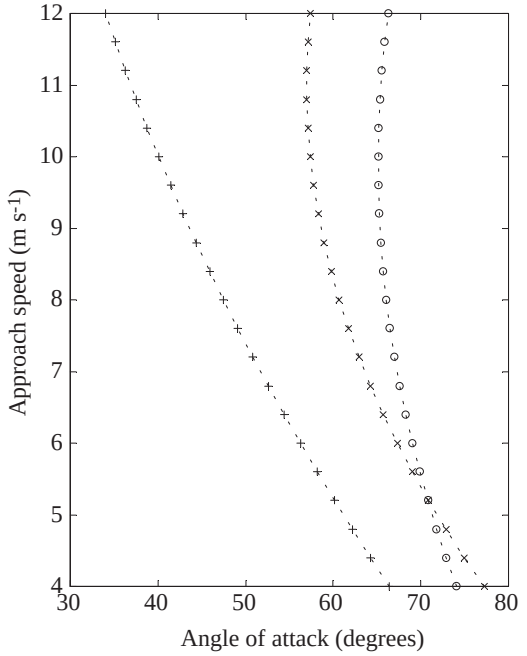

Fig. 7. Predicted optimal angle of attack for different approach velocities using (+) a spring-mass model (leg stiffness 16 kN m^{-1}), (○) the present two-segment model with one extensor muscle (see Fig. 5) and (×) the same model extended by an extensor force–length characteristic with l_{opt}=1.4l_f, where l_f is the muscle fibre length and l_{opt} is the optimal fibre length.

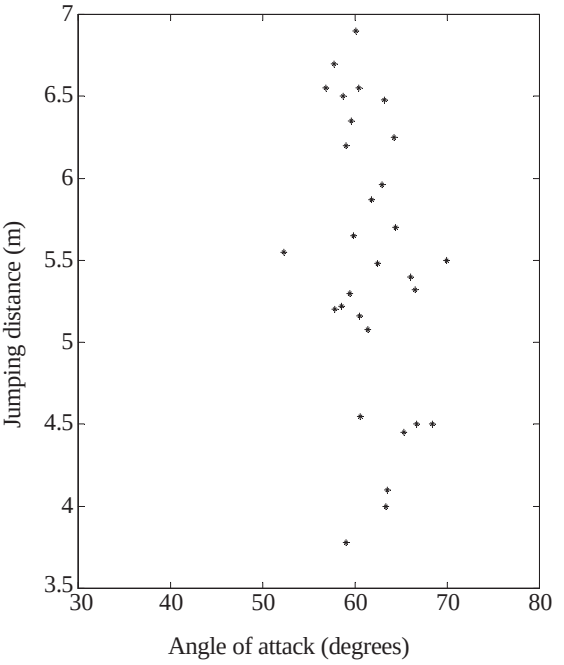

Fig. 8. Experimental analysis of variation in the chosen angle of attack with jumping distance in 30 long jumps by 18 individuals.

length l_f with respect to the optimal fibre length l_{opt}, this leads to a slightly increased dependency of the predicted optimal angle on running speed (l_f=l_{opt}/1.4 in Fig. 7). Nevertheless, for maximum performance, we assume that the muscle works at near the maximum l_f>l_{opt}/1.2 within the force–length curve.

To what extent can a highly activated knee extensor contribute to the first force peak?

How does jumping performance depend on muscle architecture? In our model, prestretch was excluded because no antagonist was present. An antagonist muscle would reduce the net knee torque. Assuming a maximum isometric force of the extensor muscle of 10 kN, a realistic preactivation of 60 % did not reproduce the high force peak observed experimentally of approximately 7–8 kN (see Fig. 2A). Only the unrealistic assumption of a completely preactivated extensor without an antagonist produced an appropriate initial peak in amplitude. The shape of this first force peak was characterised by a rapid rise followed by a steady descent similar to that described by Alexander (1990). However, the shape of the curve in Alexander's (1990) model was not due to force enhancement by eccentric operation of the muscle but was instead a direct consequence of the geometric conditions and an assumed prestretch of the series elastic component (geometry function of the leg, see equation A5; Van Ingen Schenau, 1989), which resulted in a rapid rise in ground reaction force (force increases from zero to maximum within one time step).

So, including realistic tendon properties and eccentric muscle loading in a model is not sufficient to describe the initial peak in force. To achieve this, it is necessary to include a combination of passive properties due to the distributed mass of the system (Seyfarth et al., 1999) and muscle properties.

What is the role of elastic components and eccentric force enhancement in jumping performance?

Jumping performance was not very dependent on tendon compliance. At high approach speeds, high eccentric forces are an important feature and increase the vertical momentum at the expense of mechanical energy loss. This requires stiff tendons to profit from high stretching velocities immediately after touch-down. In contrast, low tendon stiffness allows a larger amount of energy to be stored elastically and extends the period during which the activated muscle fibres are stretched. As shown in vertical jumping (Zajac, 1993), energy storage and muscle work output are compensating effects. Thinner tendons could improve mechanical efficiency but prevent muscle fibres from making use of high eccentric forces.

How does jumping performance depend on muscle architecture?

Jumping distance was more sensitive to changes in relative fibre length R_ℓ than to the ratio of tendon to muscle fibre cross-sectional areas R_A (Fig. 6). Good jumpers benefit from short muscle fibres and long tendons. This is a well-known architectural feature of animals specialised for jumping (Alexander, 1988; Ettema, 1996). Nevertheless, the optimal angle of attack was not very dependent on the actual muscle design (Fig. 6). Exactly this observation was found in an

experimental analysis of long jumpers with a variety of abilities (Fig. 8).

Furthermore, the maximum muscle velocity v_{Max} did not play a crucial role in the performance of the take-off phase because the muscle produces very little positive work (Fig. 4). Therefore, maximum performance was observed for the shortest fibres. Nevertheless, intrinsic maximum muscle velocity could have a positive influence on running speed.

Shortcomings of the model and future directions

We cannot reproduce accurately the magnitude of the first force peak because no distributed masses corresponding to those of the supporting leg were included in the present model (Seyfarth et al., 1999). This results in shorter jumps (–9 %) and somewhat flatter take-off velocity angles (–7 °) than those observed experimentally.

Furthermore, a foot is not included, and thus the sequence of impacts generated by the contact of the heel pad and the ball of the foot was not represented in our model (see Hatze, 1981). The lack of the foot also resulted in unrealistically high muscle forces and a shorter contact time (Stefanyshyn and Nigg, 1998). Furthermore, plantarflexion, swinging movements of the leg and arm lifting raise the take-off position of the body centre of mass (Hay and Nohara, 1990; Seyfarth et al., 1999).

Our model cannot simulate the details of prestretch because no antagonists are present and the segments have zero mass. In reality, preactivation before touch-down does occur (Kyröläinen et al., 1987). We compensated for this to some degree by introducing an instantaneous increase in activation state.

Very short muscle fibres require a specific muscle architecture (e.g. characterised by large pennation angles) and reduce the range of muscle lengths over which high forces can be produced (as a result of the force–length relationship). This was not included in our model.

The model could be improved by introducing other leg muscles. For example, the bi-articular gastrocnemius muscle couples knee extension to plantarflexion (Van Ingen Schenau, 1989) and improves the utilisation of the work capacity of the extensor muscle. However, the net knee torque can be increased through the simultaneous activation of other muscles not spanning the knee (e.g. hip extensors and plantar flexors) (Zajac, 1993). Inclusion of these muscles and their effects on the operation of the knee extensors awaits for further investigation.

To keep the tendon strain below the critical value for rupture, a high stiffness of the serial tendon had to be assumed. This meant that, with a fully activated muscle, spring-like sinusoidal patterns of the ground reaction force were not possible. To represent the spring-like behaviour during ground contact, additional elastic structures (deformation of the foot, Achilles tendon, ligaments) should be introduced into the model. With regard to the spring-mass model (Blickhan, 1989; Seyfarth et al., 1999), the leg can produce only a certain maximum force and therefore has a limited capacity to operate like a spring. Thus, accurate prediction of the limited take-off velocity angle of human long jumps can only be achieved by taking the muscle properties into account.

APPENDICES

Appendix 1: the force–velocity relationship of the muscle fibres

For shortening ($v_{CE} \leqslant 0$):

$$F_{CE} = F_{Max}\,\frac{v_{Max} + v_{CE}}{v_{Max} - G v_{CE}}\,, \tag{A1}$$

and for lengthening ($v_{CE} \geqslant 0$):

$$F_{CE} = F_{Max}\left(1.8 + 0.8\,\frac{v_{CE} - v_{Max}}{7.56 G v_{CE} + v_{Max}}\right), \tag{A2}$$

where v_{CE} is muscle fibre lengthening velocity, F_{CE} is muscle fibre force, F_{Max} is the maximum isometric force, v_{Max} is the maximum shortening velocity and G is a constant (here G=5) (Van Leeuwen, 1992; Otten, 1987). The maximum isometric stress of the muscle fibres σ_{Max} and their cross-sectional area A_{CE} determined the maximum isometric force F_{Max}:

$$F_{Max} = \sigma_{Max} A_{CE}\,. \tag{A3}$$

Appendix 2: stress–strain relationship of the elastic components

$$\sigma = \begin{cases} c_1 \varepsilon^{c_2} & \text{for } \varepsilon \quad \varepsilon_C \\ c_3 \varepsilon + c_4 & \text{for } \varepsilon \geqslant \varepsilon_C \end{cases}, \tag{A4}$$

where σ is stress, c_1–c_4 are constants, ε is strain and ε_C is critical strain. The elastic components behave nonlinearly until a specific critical strain $\varepsilon \leqslant \varepsilon_C$ and linearly for higher strains $\varepsilon \geqslant \varepsilon_C$. The exponent c_2 was 1.75, and the tangent modulus of the linear part c_3 was 1.5 GPa. The critical strain ε_C was 0.035 for the serial tendon and 0.1 for the parallel element (Van Leeuwen, 1992, referring to measurements of Ker, 1981). The remaining variables c_1 and c_4 are calculated from the given variables c_2 and c_3.

Appendix 3: the ground reaction force

The ground reaction force F_G caused by the muscle–tendon complex force F_{MTC} was given by:

$$F_G = r F_{MTC}/d\,, \tag{A5}$$

where r is the moment arm of the knee extensor muscle and d is the moment arm of the ground reaction force (Fig. 1). During ground contact, the equations of motion of the point mass m were:

$$\ddot{x} = -(F_G/m)\cos\alpha\,, \tag{A6}$$

$$\ddot{y} = (F_G/m)\sin\alpha - \boldsymbol{g}\,, \tag{A7}$$

where $\boldsymbol{g}$ is gravitational acceleration, α is the leg angle, and $\ddot{x}$ and $\ddot{y}$ are the horizontal and vertical accelerations, respectively.

Appendix 4: the muscle design variables

The ratios $R_A = A_f/A_t$ and $R_\ell = l_f/l_{MTC}$, where A_f and A_t are the physiological cross-sectional areas of the muscle fibres and serial tendon, respectively, and l_f and l_{MTC} are the lengths of the fibres and muscle–tendon complex, respectively, were used

to calculate the tendon cross-sectional area using the total muscle–tendon complex mass m_{MTC}, the mean density ρ_{MTC} and the total muscle–tendon complex length $l_{MTC}=l_f+l_t$, where l_t is tendon length:

$$m_{MTC} = \rho_{MTC} V_{MTC} = \rho_{MTC}(A_f l_f + A_t l_t) . \quad (A8)$$

V_{MTC} is the volume of the muscle–tendon complex. Note that the muscle pennation angle was neglected in this approach. Introducing the design variables R_A and R_ℓ, we obtain:

$$A_t = \frac{m_{MTC}}{l_{MTC}\,\rho_{MTC}} \frac{1}{R_\ell(R_A - 1) + 1} . \quad (A9)$$

At this stage, the subscript f (equation A8) denotes the muscle belly including both the parallel element and the muscle fibres themselves, whose lengths are identical. The parallel element takes up only a small part of the cross-sectional area: $A_{PE}=0.01A_f$.

Appendix 5: jumping distance

Given the take-off variables (position x_E, y_E and velocity $v_{E,x}$, $v_{E,y}$), from numerical integration, the jumping distance x_{JD} is:

$$x_{JD} = \frac{v_{E,x}}{g} (v_{E,y} + \sqrt{v_{E,y}^2 + 2g y_E}) . \quad (A10)$$

List of symbols

A_{CE}	physiological cross-sectional area of muscle fibres
A_f	physiological cross-sectional area of muscle belly (contractile element and parallel elastic component)
A_{PE}	physiological cross-sectional area of parallel elastic component (PE)
A_t	physiological cross-sectional area of serial tendon element (SE)
c_1–c_4	constants in the stress–strain relationship of the elastic elements (serial elastic component and parallel elastic component)
CE	contractile element
d	moment arm of the ground reaction force
F_{CE}	muscle fibre force
F_{ECC}	maximum eccentric force of muscle fibres
F_G	ground reaction force
$F_{G,Exp}$	experimentally measured ground reaction force (from Seyfarth et al., 1999)
$F_{G,Mod}$	modelled ground reaction force
F_{Max}	maximum isometric force of muscle fibres
F_{MTC}	muscle force
$F_{MTC,Mod}$	modelled internal muscle force
F_{PE}	force of parallel elastic element
F_{SE}	force of serial elastic element
G	constant in the Hill equation (equation A1)
g	gravitational acceleration
l	length of each leg segment
l_f	length of the muscle belly (contractile element and parallel elastic component)
l_{LEG}	leg length, distance between point of ground contact and hip
l_{MTC}	reference length of the muscle–tendon complex
l_{opt}	optimum fibre length
l_t	length of serial tendon (serial elastic component)
m	point mass at the hip
m_{MTC}	mass of muscle–tendon complex
MTC	muscle–tendon complex
N_{ECC}	eccentric force enhancement (F_{ECC}/F_{Max})
PE	parallel elastic element
r	moment arm of the patella tendon
R_A	ratio of cross-sectional areas (A_f/A_t) of the muscle
R_ℓ	relative fibre length (l_f/l_{MTC})
SE	serial elastic component
v_0	approach velocity
$v_{0,x}$	horizontal component of the touch-down velocity
$v_{0,y}$	vertical component of the touch-down velocity
v_{CE}	muscle fibre lengthening velocity
$v_{E,x}$	horizontal component of the take-off velocity
$v_{E,y}$	vertical component of the take-off velocity
v_{Max}	maximum shortening velocity of muscle fibres
V_{MTC}	volume of the muscle–tendon complex
(x,y)	horizontal and vertical coordinates of the point mass
$(\ddot{x},\ddot{y})$	second time derivative of the coordinates of the point mass
(x_E,y_E)	coordinates at take-off
x_{JD}	jumping distance
α	leg angle
α_0	angle of attack (leg angle at touch-down)
α_{opt}	optimal angle of attack resulting in maximum predicted jumping distance
ε	strain
$\dot{\varepsilon}_{Max}$	maximum muscle fibre strain rate
ε_C	critical strain dividing the non-linear and linear behaviour of the tendon
φ	knee angle
φ_0	initial knee angle at touch-down
ρ_{MTC}	density of the muscle–tendon complex
σ	stress
σ_{Max}	maximum isometric stress of muscle fibres

We thank Professor R. F. Full (Berkeley) for useful comments on a draft of this paper. This work was supported by a DAAD Doktorandenstipendium im Rahmen des gemeinsamen Hochschulsonderprogramms III von Bund und Länder to A.S. and by DFG grant Bl 236/7.

References

Alexander, R. McN. (1988). *Elastic Mechanisms in Animal Movement.* Cambridge: Cambridge University Press.

Alexander, R. McN. (1990). Optimum take-off techniques for high and long jumps. *Phil. Trans. R. Soc. Lond. B* **329**, 3–10.

Alexander, R. McN., Bennett, M. B. and Ker, R. F. (1986). Mechanical properties and functions of the paw pads of some mammals. *J. Zool., Lond.* A **209**, 405–419.

Alexander, R. McN. and Vernon, A. (1975). The dimensions of the knee and ankle muscles and the forces they exert. *J. Human Movt. Stud.* **1**, 115–123.

Blickhan, R. (1989). The spring-mass model for running and hopping. *J. Biomech.* **22**, 1217–1227.

Bobbert, M. F., Gerritsen, K. G. M., Litjens, M. C. A. and van Soest, A. J. (1996). Why is countermovement jump height greater than squat jump height? *Med. Sci. Sports Exerc.* **27**, 1012–1020.

Close, R. I. (1972). Dynamic properties of mammalian skeletal muscles. *Physiol. Rev.* **52**, 129–197.

Ettema, G. J. C. (1996). Elastic length–force characteristics of the gastrocnemius of the hopping mouse (*Notomys alexis*) and the rat (*Rattus norvegicus*). *J. Exp. Biol.* **199**, 1277–1285.

Hatze, H. (1981). A comprehensive model for human motion simulation and its application to the take-off phase of the long jump. *J. Biomech.* **14**, 135–142.

Hay, J. G. (1993). Citius, altius, longius (faster, higher, longer): The biomechanics of jumping for distance. *J. Biomech.* **26** (Suppl. 1), 7–22.

Hay, J. G., Miller, J. A. and Canterna, R. W. (1986). The techniques of elite male long jumpers. *J. Biomech.* **19**, 855–866.

Hay, J. G. and Nohara, H. (1990). Techniques used by elite long jumpers in preparation for takeoff. *J. Biomech.* **23**, 229–239.

Ker, R. F. (1981). Dynamic tensile properties of the plantaris tendon of sheep (*Ovis aries*). *J. Exp. Biol.* **93**, 283–302.

Kyröläinen, H., Avela, J., Komi, P. V. and Gollhofer, A. (1987). Function of the neuromuscular system during the last two steps in the long jump. In *Biomechanics XI-B* (ed. G. de Groot, A. P. Hollander, P. A. Huijing and G. J. van Ingen Schenau), pp. 557–560. Amsterdam: Free University Press.

Lees, A., Graham-Smith, P. and Fowler, N. (1994). A biomechanical analysis of the last stride, touchdown and takeoff characteristics of the men's long jump. *J. Appl. Biomech.* **10**, 61–78.

Luhtanen, P. and Komi, P. V. (1979). Mechanical power and segmental contribution to force impulses in long jump take-off. *Eur. J. Appl. Physiol.* **41**, 267–274.

Otten, E. (1987). A myocybernetic model of the jaw system of the rat. *J. Neurosci. Meth.* **21**, 287–302.

Pandy, M. G., Zajac, F. E., Sim, E. and Levine, W. S. (1990). An optimal control model for the maximum-height human jumping. *J. Biomech.* **23**, 1185–1198.

Pierrynowski, M. R. (1985). A physiological model for the evaluation of muscular forces in human locomotion: theoretical aspects. *Math. Biosci.* **75**, 69–101.

Seyfarth, A., Friedrichs, A., Wank, V. and Blickhan, R. (1999). Dynamics of the long jump. *J. Biomech.* **32**, 1259–1267.

Spector, S. A., Gardiner, P. F., Zernicke, R. F., Roy, R. R. and Edgerton, V. R. (1980). Muscle architecture and force–velocity characteristics of cat soleus and medial gastrocnemius: implications for motor control. *J. Neurophysiol.* **44**, 951–960.

Stefanyshyn, D. J. and Nigg, B. M. (1998). Contribution of the lower extremity to the mechanical energy in running vertical jumps and running long jumps. *J. Sports Sci.* **16**, 177–186.

Van Ingen Schenau, G. J. (1989). From rotation to translation: constraints on multi-joint movements and the unique action of bi-articular muscles. *Human Movt. Sci.* **8**, 301–337.

Van Leeuwen, J. L. (1992). Muscle function in locomotion. In *Advances in Comparative and Environmental Physiology 11: Mechanics of Animal Locomotion* (ed. R. McN. Alexander), pp. 191–242. Heidelberg, Berlin: Springer-Verlag.

Winters, J. M. and Woo, S. L.-Y. (1990) (eds). *Multiple Muscle Systems: Biomechanics and Movement Organization.* New York: Springer Verlag.

Witters, J., Bohets, W. and Van Coppenolle, H. (1992). A model of the elastic take-off energy in the long jump. *J. Sports Sci.* **10**, 533–540.

Zajac, F. E. (1993). Muscle coordination of movement: a perspective. *J. Biomech.* **26** (Suppl. 1), 109–124.